Dynamic state-space estimation based fault characterization algorithm

Gregor Becker*, Johann Jaeger†
Insitute of Electrical Energy Systems
Friedrich-Alexander-Universität Erlangen-Nürnberg
Erlangen, Germany
Email: *gregor.becker@fau.de, †johann.jaeger@fau.de

Matthias Kereit
Smart Infrastructure
Siemens AG
Berlin, Germany
Email: matthias.kereit@siemens.de

***Abstract*—The increasing provision of electrical energy in electrical power grids and their growing converter infeed with unpredictable distorted short-circuit currents, increase the criticality of outages in this area. Consequently, such outages must be minimized to maintain high reliability and service quality. Within the literature, two concepts are identified as essential to mitigate extended outages: enhanced system monitoring and the rapid, accurate characterization of both fault location and type.**

This paper presents a novel algorithm for fault characterization that exhibits inherent robustness to non-ideal sinusoidal signals and modeling inaccuracies due to its comparative decisions. The approach relies on sampled values provided to a centralized IED in accordance with the IEC 61850 standard. Thus, representing a reasonable use case of the new available centralized data. The algorithm is derived analytically and validated through a proof-of-concept simulation. The results highlight the algorithm's enduring robustness, enabling precise fault characterization well below the first cycle without dependence on phasor formation.

***Index Terms*—power system protection, fault localization, dynamic state-space estimation, kalman-filter**

I. Introduction

A. Background

The increasing provision of electrical energy in electrical power grids and their growing converter infeed with unpredictable distorted short-circuit currents, increase the criticality of outages in this area. Consequently, these outages should be kept as short as possible in order to maintain high reliability and service quality. [1], [2] To achieve this, on the one hand a higher level of monitoring of the current system through digital centralized available measurement data is required [1]. On the other hand, a fast and reliable fault characterization is necessary, including both the fault type and the approximate fault location [1], [4]. Both the usage of the new available data and the fault characterization are part of the presented algorithm and thus representing a reasonable use case.

While fault characterization itself does not directly enhance the monitoring of distribution networks (DNs), the increasing establishment of digital and centralized available measurement data opens up new opportunities for improving fault characterization algorithms (FCAs) [2], [4]. Furthermore, DNs are evolving from passive power system components to "active" DNs [2]. This new level of flexibility creates a gap in the development and investigation of new FCAs [2].

B. Literature Review

Currently, considerable effort is being invested in developing methods that leverage the new degrees of freedom available for the fault characterization in "active" DN. This new designs of FCAs can be devided in two main categories, which can in turn be subdivided in different approaches. The two main categories are, on the one hand, *signal-analysis-based* and, on the other hand, *knowledge-based* FCAs. *Knowledge-based* algorithms can be futher classified into artificial neural networks, fuzzy logic, and other machine learning approaches [2]; however, these are not of further interest for this contribution. Travelling Wave [2] – [4], synchrophasors [1] – [5], [7] and sampled values (SVs) [4], [6] can be grouped under the second category, namely *signal-analysis-based* FCAs, which are systematically illustrated in a simplified overview in Fig. 1.

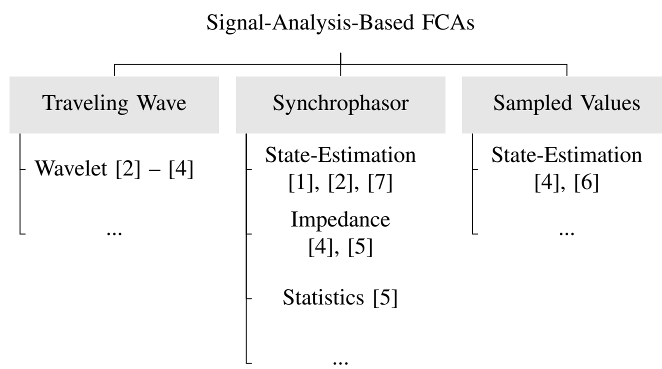

Fig. 1. Current investigations on signal-analysis-based fault characterization algorithms (does not claim to be complete).

Synchrophasor-based methods are currently receiving the most attention, as their capacbility to evaluate the data of phase measurement units (PMUs) aligns their increasing establishment. Several contibutions analyze the potential of advanced, impedance-based FCAs [4], [5], while others investigate dynamic state estimation-based FCAs [1], [2], [7]. Nevertheless, synchrophasor-based FCAs must address the issue that phasor calculation filters out the transient information of the signals [4]. This drawback of phasors and the fact that converters increasingly provide non-ideal sinusoidal currents and voltages have prompted both Liu et al. [4] and Chen et al. [6] to investigate SV dynamic state estimation-based FCAs. They

979-8-3315-8138-1

observeed an immunity to higher harmonics, low short-circuit currents, and zero and negative sequence components [6].

C. Motivation & Contributions

The potential of SV dynamic state estimation FCAs is significant and has not been fully realized by the approaches presented by Liu et al. [4] and Chen et al. [6]. Thus, this contribution introduces and demonstrates an alternative approach. Unlike existing approaches, it does not use pseudo measurements (e.g. the resulting current of a power system demand estimation [4]). This makes the model deterministic and more secure, but severely limits its size of the investigated area of interest (AOI). The goal of this contribution is to establish a foundation for future research in the area FCAs based on dynamic state-space estimation (DSSE).

D. Paper Organization

The remainder of the paper ist organized as follows. In section II the DSSE-based FCA is derived and its functionality is described. Afterwards the investigated power system and AOI of the proof of concept case study is presented in section III. The simulation results are presented in section IV, and discussed in section V. Finally the findings are summarized in section VI.

II. Methodology

This contribution investigates a newly developed signal-analysis-based FCA which utilizes SVs and DSSE. Thus the DSSE using Kalman-Filters (KFs) is described first. Subsequently, the new approach for DSSE-based FCA is presented, and its decision criterion for both the fault location and fault type is derived. Finally, the derivation of a state-space model of a single-line-to-ground (SLG) fault is exemplarly demonstrated.

A. Dynamic state-space estimation

As implied by the name, the DSSE relies on a state-space model, which is provided in linear form in Fig. 2 and in (1) and (2).

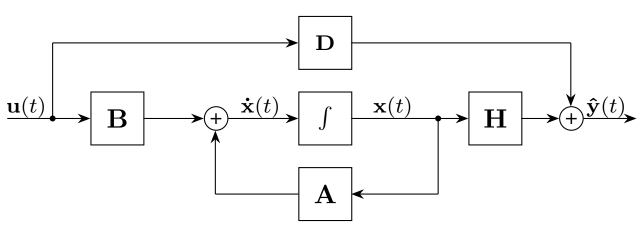

Fig. 2. Principal diagramm of a state-space model [8].

$$\mathbf{x_p}(t) = \mathbf{A} \cdot \mathbf{x_c}(t-1) + \mathbf{B} \cdot \mathbf{u}(t) \tag{1}$$

$$\hat{\mathbf{y}}(t) = \mathbf{H} \cdot \mathbf{x_p}(t) + \mathbf{D} \cdot \mathbf{u}(t) \tag{2}$$

Therein $\mathbf{A}$, the system matrix, represents the relationship between the current calculated and the previous sample, disregarding the effect of external influences ($\mathbf{u}(t)$). While the input matrix $\mathbf{B}$ accounts for these external influences. The matrix $\mathbf{D}$, also referred to as transition matrix, can be neglected and consequently set to $\mathbf{0}$ since the signals of the electrical power systems cannot exhibit instantaneous changes. Finally, the observation matrix $\mathbf{H}$, is used to extract the measured entries of the state-space vector $\mathbf{x_p}(t)$. [8] Adding a state-space estimation algorithm, such as a time-invariant linear KF, enables the dynamic estimation process to optimally balance between the estimates against the real-world power system measurements. The feedback, or innovation term ($\mathbf{y}(t) - \mathbf{H} \cdot \mathbf{x_p}(t)$), is multiplied by the Kalman gain $\mathbf{K}$ and subtracted from the model's estimate (see (3)). [9]

$$\mathbf{x_c}(t) = \mathbf{x_p}(t) - \mathbf{K} \cdot (\mathbf{y}(t) - \mathbf{H} \cdot \mathbf{x}_\mathrm{p}(t)) \tag{3}$$

Through this feedback mechanism, the DSSE algorithm compensates the unknown initial system state and attenuates both measurement noise and modeling errors.

B. Algorithm and Decision Criterion of the DSSE-based FCA

Each state-space model corresponds to a specific power system topology or condition, such as faulted or unfaulted state of a component. Accordingly, a library of models can be constructed to represent all notable faults that might occure along a transmission line. These models are generated by varying the *fault position*, *fault resistance*, and *fault type* (e.g., non-resistive single-line-to-ground fault at 50 % of the line length). By implementing these models within a parallel estimation framework, it becomes possible to simultaneously estimate and extract all potential fault scenarios measured extract of the state-space vector ($\mathbf{y}(t)$). The outputs are then compared with the measured system states of the physical power system (see Fig. 3).

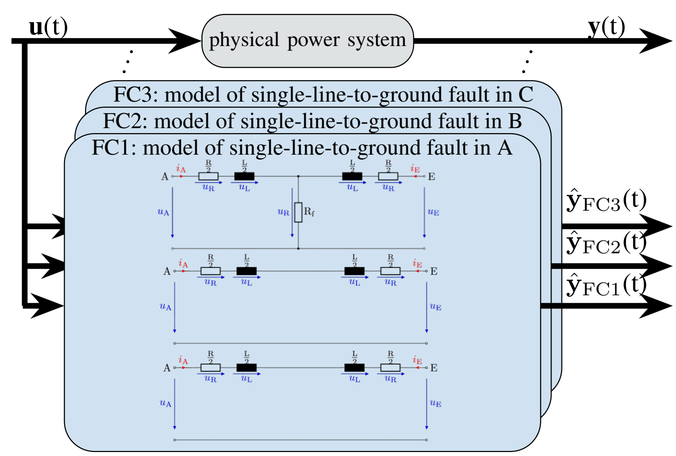

Fig. 3. Exemplary parallel structure of the investigated FCA.

As can be observed, the fault representation in the three-phase power system (ABC representation) serves as the foundation for constructing the corresponding state-space model. Once the system state is estimated for each model, the next step is to determine which models matches the actual system behavior the best. To achieve this, a decision criterion based on the *normalized quadratic Euclidean norm* is employed (see (4)). This metric quantifies the deviation between the measured

979-8-3315-8138-1

and estimated system outputs, allowing the identification of the model (*fault type*, *fault resistance* & *fault position*) with the minimum error as the most representative.

$$\mathrm{FC}_i = \frac{\min(\|\mathbf{y}(t)-\hat{\mathbf{y}}_i(t)\|_2)}{\|\mathbf{y}(t)-\hat{\mathbf{y}}_i(t)\|_2} \tag{4}$$

Finally, the proposed algorithm requires a triggering mechanism, which, for simplicity, is defined as a drop below the decision threshold of the algorithm presented in [9], indicating the occurrence of a fault or another topological change.

C. Derivation of a SLG fault state-space model

To illustrate the development of the state-space models, the case of a SLG fault in phase C is presented. For this purpose, the corresponding three-phase equivalent fault-network is established (see Fig. 4). In all state-space models considered, the line-to-ground capacitances are neglected to maintain system observability and simplify the model structure [10].

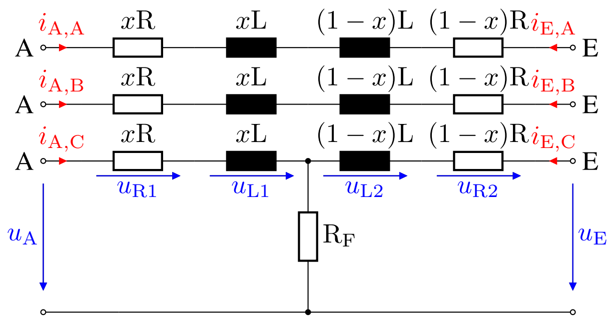

Fig. 4. Three phase equivalent circuit of a SLG fault in C.

Evaluating the three-phase network allows the derivation of the fault conditions, electric quantities at fault location, given in (5).

$$\begin{array}{ll} \underline{\text{Currents}} & \underline{\text{Voltages}} \\ i_{\mathrm{F,A}} = 0 & u_{\mathrm{F,A}} \neq 0 \\ i_{\mathrm{F,B}} = 0 & u_{\mathrm{F,B}} \neq 0 \\ i_{\mathrm{F,C}} = i_{\mathrm{A,C}} + i_{\mathrm{E,C}} & u_{\mathrm{F,C}} = i_{\mathrm{F,C}} \cdot \mathrm{R_F} \end{array} \tag{5}$$

The next step in the modelling process is the application of the Clarke transformation, which is based on Edith Clarke's transformation equations [11]. This transformation converts the three-phase quantities from the ABC into the $\alpha\beta0$ representation, facilitating the decoupled analysis of the system components. The corresponding currents and voltages expressed in the Clarke frame are shown in (6), and the resulting Clarke fault network representation is illustrated in Fig. 5.

$$\begin{aligned} i_0 &= \tfrac{1}{3}(i_{\mathrm{F,A}} + i_{\mathrm{F,B}} + i_{\mathrm{F,C}}) &&= \tfrac{1}{3} i_{\mathrm{F,C}} \\ i_\alpha &= i_{\mathrm{F,A}} - i_0 &&= -i_0 \\ i_\beta &= (\tfrac{1}{\sqrt{3}} i_{\mathrm{F,B}} - \tfrac{1}{\sqrt{3}} i_{\mathrm{F,C}}) &&= -\tfrac{1}{\sqrt{3}} i_{\mathrm{F,C}} = -\sqrt{3} i_0 \\ u_0 &= \tfrac{1}{3}(u_{\mathrm{F,A}} + u_{\mathrm{F,B}} + u_{\mathrm{F,C}}) &&= \tfrac{1}{2} u_\alpha + \tfrac{\sqrt{3}}{2} u_\beta + 3 i_0 \mathrm{R_F} \\ u_\alpha &= \tfrac{2}{3} u_{\mathrm{F,A}} - \tfrac{1}{3} u_{\mathrm{F,B}} - \tfrac{1}{3} u_{\mathrm{F,C}} \\ u_\beta &= \tfrac{1}{\sqrt{3}} u_{\mathrm{F,B}} - \tfrac{1}{\sqrt{3}} u_{\mathrm{F,C}} \end{aligned} \tag{6}$$

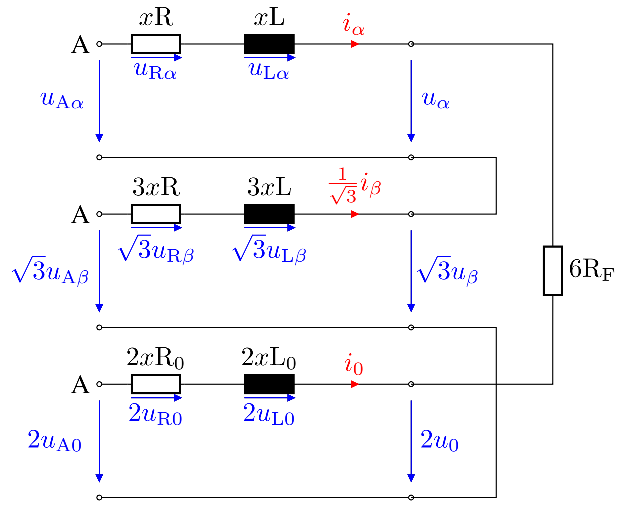

Fig. 5. Clarke fault network representation.

By evaluating Kirchhoff's voltage and current law in the interconnected Clarke component networks, the state-space model of the SLG fault in phase C is obtained. As an example, the ordinary differential equation (ODE) describing the α-component sending-end current is presented in (7).

$$\begin{aligned} \frac{di_\alpha}{dt} &= \frac{(u_{\mathrm{A}\alpha} + \sqrt{3}u_{\mathrm{A}\beta} - 2u_{\mathrm{A0}})}{(4x\mathrm{L} + 2x\mathrm{L_0})} \\ &\quad - \frac{(2\mathrm{R} + \mathrm{R_0} + \frac{3}{x}\mathrm{R_F})}{(2\mathrm{L} + \mathrm{L_0})} \cdot i_{\mathrm{A}\alpha} - \frac{\frac{3}{x}\mathrm{R_F}}{(2\mathrm{L} + \mathrm{L_0})} \cdot i_{\mathrm{E}\alpha} \end{aligned} \tag{7}$$

Repeating this procedure for $i_{\mathrm{E}\alpha}$, $i_{\mathrm{A}\beta}$, $i_{\mathrm{E}\beta}$, i_{A0}, i_{E0} in the remaining Clarke component networks yields the complete state-space model for the DSSE of a SLG in phase C. By applying the same procedure to all relevant fault types, the library of models required for the FCA is constructed.

III. Case Study as Proof of Concept

Following the formulation of the proposed algorithm, the derivation of its corresponding models, and the definition of its decision criteria, a proof-of-concept study is conducted. For this purpose, a simulation on a representative power system is carried out. To this end, the topology shown in Fig. 6 is implemented in DIgSILENT PowerFactory. Within this network, Line2-3 represents the AOI for both the FCA as well as the fault identification algorithm (FIA), which serves as the trigger mechanism for the FCA.

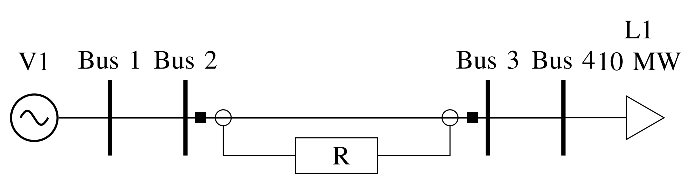

	R (Ω)	X (Ω)	$\mathrm{R_0}$ (Ω)	$\mathrm{X_0}$ (Ω)	U_n (kV)
Line1-2	1.57	3.19	3.01	15.33	20
Line2-3	31.4	63.8	60.27	306.65	20
Line3-4	1.57	3.19	3.01	15.33	20

Fig. 6. Single-line diagram of the investigated network topology (adapted from [9]).

979-8-3315-8138-1

IV. Simulation results

An electromagnetic transient (EMT) simulation of the network topology is performed in PowerFactory. A zero fault resistance SLG fault in phase C is applied at 25 % of the line length – corresponding to 5 km from Bus 2. The fault is initiated at 2.5 s into the simulation, and the simulation is terminated at 5 s. Throughout the investigation, all instrument transformers are assumed to be ideal, such that they do not affect the sinusoidal waveform (e.g., due to saturation) or the temporal synchronization (e.g., due to merging unit latency). A sampling rate of 4 kHz, corresponding to a sampling interval of 0.00025 s, is used. The resulting time-domain data are subsequently exported for use in the FIA and thereafter, in the FCA, both implemented in Python.

A. Results of the fault identification algorithm

Next, the trigger time of the newly developed FCA is determined. To this end, the FIA described in [9] is employed with the parameters listed in TABLE I.

TABLE I
Fault identification algorithm Kalman-Filter data.

Parameter	Value
Measurement noise covariance matrix $\mathbf{R}$	$0.2{\cdot}\mathbf{I}$
Process noise covariance matrix $\mathbf{Q}$	$3{\cdot}\mathbf{I}$
Weighting matrix of GSQR $\mathbf{W}$	$15{\cdot}\mathbf{I}$

Fig. 7 illustrates the confidence level (p-Value) obtained from the FIA simulation. This p-Value serves as the triggering mechanism for the investigated FCA. Prior to the fault occurence, the p-Value remains approximately constant at 1, indicating normal system operation. Following the fault initiation at 2.5 s, the p-Value decreases sharply and reaches 0 after 0.0005 s / 2 samples. During this decrease, it crosses the triggering threshold $\alpha = 0.8$, which represents the trigger event for the FCA. Throughout the remainder of the simulation, the p-Value does not exceed the threshold again. Consequently, the FCA investigation should begin with the time series starting at 2.50025 s (first sample below the threshold) in the simulation.

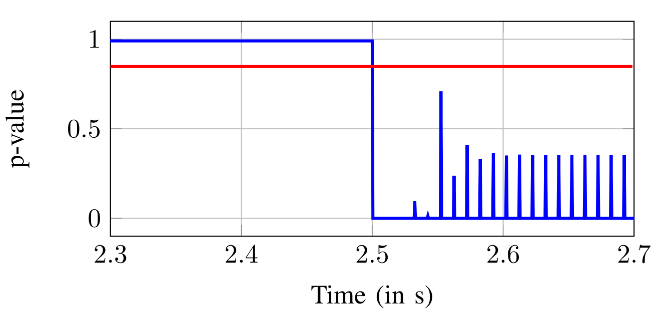

Fig. 7. Confidence niveau of the fault identification algorithm.
Legend: blue: p-Value, red: Triggering threshold.

B. Results of the fault characterization algorithm

The FCA is applied to the time series starting from the triggering event at 2.50025 s in the simulation. Both the measurement and the process noise covariance matrix are set to $1 \cdot \mathbf{I}$. The algorithm provides several result representations. On the one hand, the time series of the Euclidean norm, as well as the estimated currents, can be visually analyzed to identify the model that best represents the current system state. On the other hand, an interactive heat map displaying the $\mathrm{FC_i}$ of each fault type for each sample enables an intuitive visualization of both the fault type and its location. Fig. 8 represents three estimated α-component network currents obtained from the DSSE of the SLG fault models for AG, BG and CG within the FCA. All estimated currents start at approximately zero due to the cold start of the KF, which assumes unknown initial conditions. Throughout the time series, deviations between these α-component currents become observable, arising from differences in the state-space representation of the individual fault types.

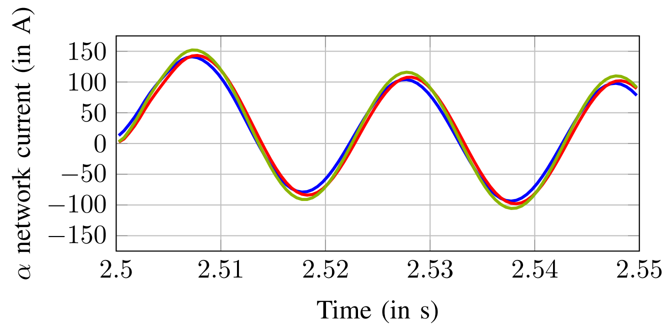

Fig. 8. Estimated α network current of the CT at Bus 2.
Legend: blue = AG DSSE, red = BG DSSE, green = CG DSSE.

Fig. 9 shows the heatmap of the 100th sample following the fault occurence, which is the second possible result format.

Fault type \ Position (in %)	1	25	50	75	99
Healthy	6	6	6	6	6
AG ($\mathrm{R_F} = 0\ \Omega$)	3	5	5	5	0
BG ($\mathrm{R_F} = 0\ \Omega$)	0	3	4	2	0
CG ($\mathrm{R_F} = 0\ \Omega$)	0	100	11	8	5
AB ($\mathrm{R_F} = 0\ \Omega$)	0	2	3	2	0
AC ($\mathrm{R_F} = 0\ \Omega$)	0	4	7	4	0
BC ($\mathrm{R_F} = 0\ \Omega$)	0	1	2	2	0
ABG ($\mathrm{R_F} = 0\ \Omega$)	0	1	2	1	0
ACG ($\mathrm{R_F} = 0\ \Omega$)	0	1	2	1	0
BCG ($\mathrm{R_F} = 0\ \Omega$)	0	1	2	4	5
ABCG ($\mathrm{R_F} = 0\ \Omega$)	0	1	2	1	0

Fig. 9. Heatmap of all non-resistive fault types of the 100th sample.

Both the color scale and the numerical values indicate that, for this sample, the SLG fault in phase C at 25 % of the line exhibits the lowest Euclidean norm and, consequently,

979-8-3315-8138-1

the highest $\mathrm{FC_i}$. Furthermore, it can be observed that no other fault type attains an $\mathrm{FC_i}$ value within 10 % of the best-fitting state-space model.

V. Discussion

A. Functionality of the new fault characterization algorithm

The functionality of the newly developed FCA was demonstrated using a simplified example topology. The FIA presented in previous work [9] identified the fault occurence quickly (1 sample after occurence) and reliably (no exceedance of the detection threshold thereafter). Thus it serves as a suitable triggering mechanism for the FCA, enabling a timely activation of the classification process. It should be noted, that in the FIA implementation used here, the optimality of the employed KF was not a focus of the investigation. The filter parameters were chosen heuristically rather than being optimized for noise characteristics or system dynamics. Consequently, the FIA's role in this study was limited to providing a functional and reproducible trigger, rather than to achieving optimal estimation performance.

During the evaluation of the FCAs results, a few isolated samples were observed in which the fault location was estimated to be approximately 25 % further along the line than the actual fault position. Nevertheless, over the entire time series, these deviations remain sporadic and statistically insignificant, indicating that the FCA produces consistent and accurate fault localization and classification results overall.

B. Robustness against non-ideal sinusoidal signals

The fact that the FCA under investigation does not rely on phasor formation implies that it can also be applied to non-ideal sinusoidal signals. Such signals may result from inverter infeeds (causing higher harmonics) or from transient power system processes (e.g., transformer inrushes outside the AOI). This assumption is supported by the findings of Chen et al. [6], who demonstrated that sample-based methods exhibit robustness against waveform distortions and deviations from pure sinusoidal behavior. A comprehensive evaluation of the presented FCA under non-ideal sinusoidal operating conditions is currently planned as part of future work.

C. Current limitations

The presented method is currently subject to two main limitations. First, it requires time-synchronized time-series data with a sampling rate of at least 4 kHz (minimum requirement of IEC 61850) to be available at a centralized measurement point, such as a centralized intelligent electronic device (IED). This prerequisite implies the widespread deployment of digital switchgear compliant with IEC 61850, as well as reliable communication between distributed measurement units and a central IED located near the SCADA system. Both conditions are not yet fully met in current power system infrastructures, which restricts the practical applicability of the proposed algorithm under the present level of digitization. Second, the method requires system observability within the state-space representation, which currently limits AOI to a single line section and therefore necessitates a high density of measurement points. Ongoing research, however, is focused on expanding the AOI through improved modeling techniques.

VI. Conclusion

A newly developed fault characterization algorithm (FCA), with its functional principle, decision criterion was presented, and its model basis was derived and discussed in detail. As a proof-of-concept, a single-line-to-ground fault in a simplified network topology was simulated using DIgSILENT PowerFactory, and the resulting FCA decisions were subsequently evaluated. The investigation demonstrated that the previously proposed fault identification algorithm (FIA) is suitable as a triggering mechanism for the FCA. Moreover, it was shown that the FCA identifies both the fault type and fault location quickly and reliably. Due to space constraints, the evaluation of the fault resistance estimation functionality was not included in this contribution. Currently, the usability of the proposed algorithm is restricted by the system observability within the state-space representation and by the limited deployment of IEC 61850-compliant digital substations. Nonetheless, the results confirm the feasibility and robustness of the proposed approach, laying the foundation for further research on fault resistance assessment, broader observability, and real-world implementation. Additionally, the use of more complex state space estimation algorithms than the linear time-invariant Kalman filter is conceivable and will be part of future investigations.

References

[1] K. Hu, Y. Cai, Z. Cai, X. Li, B. Cen, Y. Chen, "Fault location method based on structure-preserving state estimation for distribution networks" IET Generation, Transmission & Distribution, vol. 15, Aug. 2022.

[2] M. Gholami, A. Abbaspour, M. Moeini-Aghtaie, M. Fotuhi-Firuzabad, M. Lehtonen, "Detecting the Location of Short-Circuit Faults in Active Distribution Network Using PMU-Based State Estimation" IEEE Transactions on Smart Grid, vol. 2, Mar. 2020.

[3] L. Shang, G. Herold, J. Jaeger, R. Krebs, A. Kumar, "High-speed fault identification and protection for HVDC line using wavelet technique" 2001 IEEE Porto Power Tech Proceedings, Sep. 2001.

[4] Y. Liu, A.P. Sakis Meliopoulos, Z. Tan, L. Sun, R. Fan, "Dynamic state estimation-based fault locating on transmission lines" IET Generation, Transmission & Distribution, vol. 17, Nov. 2017.

[5] S. Pandey, A. K. Srivastava, B. G. Amidan, "A Real Time Event Detection, Classification and Localization Using Synchrophasor Data" IEEE Transactions on Power Systems, vol. 6, Mar. 2020.

[6] Z. Chen, S. Cai, D. Lu, A. P. Sakis Meliopoulos, "Time Domain Distribution System Fault Location based on Dynamic State Estimation" 2024 IEEE Power & Energy Society General Meeting (PESGM), Jul. 2024.

[7] Y. Liao, M. Kezunovic, "Optimal Estimate of Transmission Line Fault Location Considering Measurement Errors" IEEE Transactions on Power Delivery, vol. 3, Jul. 2007.

[8] R. Marchthaler, S. Dingler, "Kalman-Filter: Einführung in die Zustandsschätzung und ihre Anwendung für eingebettete Systeme" Springer Fachmedien Wiesbaden, 2017, 2nd edn. 2024.

[9] G. Becker, G. Kordowich, J. Jaeger, "Model-based power system protection – benefits and drawbacks" IET Conference Proceedings, vol. 5, Apr. 2025.

[10] Z. Yun, T. Wen, C. Wang, "Fault Location Method for Three-Terminal Lines in Distribution Network Based on Line Voltage Measured by μMPMU" IEEE Transactions on Smart Grid, vol. 12, Nov. 2021.

[11] E. Clarke, "Circuit Analysis of AC Power Systems" Wiley, vol. I, 1943.